https://doi.org/10.20965/ijat.2019.p0382

Paper:

Modeling Approach for Estimation of Contact and Friction Behavior of Rolling Elements in Linear Bearings

Matthias Reuss*,†, Taku Sakai, and Atsushi Matsubara*****

*Makino Milling Machine Co., Ltd.
4023 Nakatsu, Aikawa-machi, Aiko-gun, Kanagawa 243-0303, Japan
†Corresponding author, E-mail: reuss.matthias@makino.co.jp
**Kyoto Works, Mitsubishi Electric, Kyoto, Japan
***Department of Micro Engineering, Kyoto University, Kyoto, Japan

[Received September 1, 2017; accepted January 15, 2019]

The improvement in the positioning accuracy of machine tools necessitates reliable friction models for compensation. Friction and damping are primarily caused by mechanical contacts, and they have a wide influence on the dynamics of machine tools. Particularly in the linear motor driven axis, linear bearings induce majority of the friction; contact is observed between the ball and raceway in linear bearings. Based on the Hertzian contact theory and a tangential force model, a model is developed for the friction behavior during the contact between the ball and raceway. This model determines the stick and slip areas, and the relative velocity at the contact surface. Hence, the calculation of the friction force, its hysteresis characteristics, and the stick and slip portions becomes possible.

Keywords: linear bearing, rolling friction, micro contact simulation, sticktion, tribology

1. Introduction

Improvements in the potential of machine tools enforce computer-aided construction and simulation tools. The desired positioning accuracy of high- and ultra-precision machine tools in micro- and nanometer range can only be achieved by accurate and reliable friction models for compensation algorithms. The mechanical behavior of all components except damping and friction is either available in the literature or can be measured directly. However, friction and damping are mainly caused by contacts, and are therefore observable only after the assembly. In particular, for linear motor driven high- and ultra-precision machine tools, the friction visible at the velocity reversal points of circularity test is primarily caused by linear bearings. The estimation and modeling of friction in bearings, and especially at the contact surface of the ball and raceway, are being researched by various scientists for decades [1–4].

This paper describes the modeling and examination of dry friction during the contact between the ball and raceway of linear bearings. While Tanaka et. al. used a single bristle model to estimate the friction for improvement of position control [5], Al-Bender et al. presented a generalized Maxwell-slip model [6, 7], which allows modeling the hysteresis behavior. It consists of multiple elementary Maxwell-slip friction models describing the discrete friction behavior in the direction perpendicular to the motion. It allows to model complex systems such as the friction in linear guideways, which depend on the traveling distance described by Futami et al. [8]. Hence, the spring-like behavior in sub-micrometer range, nonlinear-spring behavior in sub-millimeter to sub-micrometer range, and Coulomb behavior in sub-millimeter range can all be modeled. In the model used in this study, both the presliding displacement, which is required to predict interactions between stiffness and stick-slip amplitude, and the frictional memory, which is essential to predict small displacements while sticking, are covered [9]. However, here the stop of movement is assumed to be infinitesimally short, which implies that the sticktion force will be constant. In this paper, firstly, the geometry of the raceway and ball, and the forces acting on them are explained. Secondly, the used friction model and its effects are described in detail. This includes the determination of stick-slip boundary, as well as the calculation of the lines of pure rolling. Thirdly, a comparison between the measurements and simulation results is made. Finally, a conclusion and an outlook to future work are provided.

This paper focuses on the theoretical examination of rolling contact and leads to a deeper understanding of the friction behavior in the contact area of rolling bodies in bearings. Furthermore, it provides a better comprehension of the contact behavior and improves friction models for simulation and compensation. This is particularly interesting for linear motor-driven high- and ultra-precision machine tools. A more detailed discussion of the measuring results is presented by Matsubara et al. [10].

2. Geometry of Ball and Raceway

The geometry of the ball and raceway, and the preload are determined using a linear bearing with cylindrical raceways. With the geometry and external force affect-

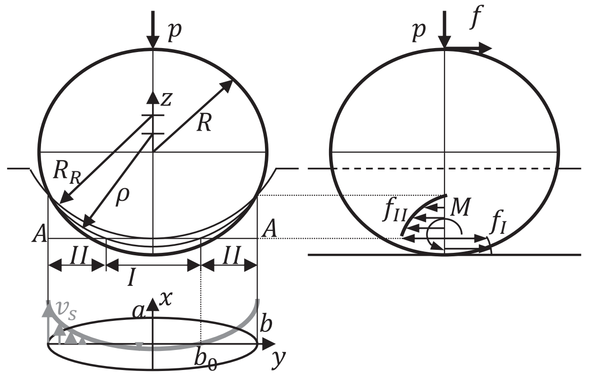

Fig. 1. Schematic representation of geometry of the ball and raceway in front and side views, and contact area in top view. The lines of pure rolling, which are characterized by the disappearance of relative velocity between the ball and raceway, can be observed. These lines are the border between the areas I and II. Furthermore, the signs of the relative velocity and the friction force are changing here. Here, the direction is the moving direction; therefore, the minor radius of the contact ellipse is a, and the major radius is b. The lowest part shows the distribution of friction force F_R with its sign corresponding to the velocity.

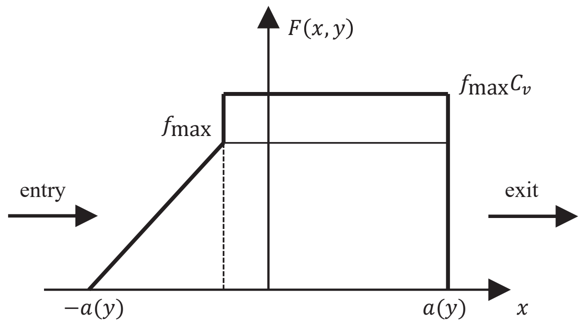

Fig. 2. Friction model with a linear slope of the friction force from entry of bristle until the maximum force $f_{\max}$. Thereafter, constant force increased by the factor C_v persists in the slipping area.

ing the carriage, contact pressure and elliptic contact surface can be calculated using the Hertzian contact theory. Therefore, only the four radii of the ellipsoidal contact surfaces, material constants, and the normal force are necessary for the calculation. For isotropic homogeneous material, as we assume in this study, these are the Young's modulus E and Poisson's ration ν [3, 11–14]. The geometry and labeling of the ball, raceway, and contact surface are schematically shown in the front, side, and top views in **Fig. 1**. Furthermore, the relative velocity v_s between the ball and raceway, and the friction force F_R are displayed in grey in the top view. The velocity inversion at the contact surface is apparent from the figure, where there are two lines of zero relative velocity and a change in sign between the areas I and II.

3. Friction Model

To describe the friction force $F(x,y)$, the contact ellipse is cut into infinitesimal stripes in the y-direction. Due to the different radii of the ball and groove, each of these stripes has a different differential velocity $v_s(y)$ [15]. For each of these stripes of the contact area, a simple general approach described by Soda [16] and used by Kimura [17] has been selected, which assumes a linear increase in the force caused by the displacement of the contacting surfaces with respect to each other, until a maximum force $f_{\max}$ is reached. Thereafter, the force stays constant, increased by the constant C_v, until the bristle leaves the contact ellipse.

$$F(x,y) = \begin{cases} k_q u(x,y)xy, & \text{if } F \leq f_{\max} \\ C_v f_{\max}, & \text{otherwise} \end{cases} \quad . \; . \; . \quad (1)$$

The contact stiffness k_q is estimated using the material parameters. This value is the substitute of Young's modulus E^* representing the contact surface of two different materials, calculated with the Young's modulus E_i and Poisson's ratio ν_i of each material, as described by the Hertzian theory.

$$k_q = E^* = \frac{1}{\frac{1}{2}\left(\frac{1-\nu_1^2}{E_1} + \frac{1-\nu_2^2}{E_2}\right)} \quad . \; . \; . \; . \; . \quad (2)$$

The used friction model, as described in Eq. (1), is shown in **Fig. 2** with the entry of the bristles at the left side and their exit at the right side.

The maximum force $f_{\max}$ is obtained from the pressure $p(x,y)$ distribution of the Hertzian contact-stress theory. The maximum tangential force is assumed to be proportional to the normal force Q at $x = 0$. The proportionality constant is the friction coefficient μ. It is determined by measuring the dry and viscous friction, and a and b are the major and minor radii of the contact ellipse.

$$p(x,y) = \frac{3}{2}\frac{Q}{\pi ab}\sqrt{1 - \frac{x^2}{a^2} - \frac{y^2}{b^2}} \quad . \; . \; . \; . \; . \; . \quad (3)$$

$$f_{\max}(y) = \mu p(x=0,y) \quad . \; . \; . \; . \; . \; . \; . \; . \; . \quad (4)$$

The position $y = \pm b_0$ is the instantaneous center of rotation, which indicated the two lines of pure rolling without slipping and translational velocity. Considering symmetry in the y-direction, it is only necessary to discuss one half of the contact ellipse. In the following sections, the positive half of the ellipse is analyzed.

3.1. Integration Intervals

Before calculating the torque, the integration intervals have to be determined, first in the x- and then in the y-direction. The boundary for the integration over x is the boundary of the contact ellipse described by Eq. (5).

$$x = \pm\frac{a}{b}\sqrt{b^2 - y^2} \quad . \; . \; . \; . \; . \; . \; . \; . \; . \; . \; . \; . \quad (5)$$

To determine the interval in the x-direction, the transition curve from stick to slip has to be calculated. Therefore, the maximum displacement u_{max} of the bristles before the occurrence of slipping has to be calculated first. This is related to the maximum force by the bristle stiffness k_q, and its sign depends on the position of the line of pure rolling b_0.

$$u_{\max} = \mathrm{sgn}(b_0 - y)\frac{f_{\max}(y)}{k_q} \quad \text{. . . . . (6)}$$

As described in Soda's and Kimura's friction model [16, 17] used by Fujita [18], the displacement of the bristles is assumed to be linearly increasing in the stick area of the contact. The gradient ξ is the relative velocity between the carriage velocity v_d and the velocity in the contact v_s. It depends on the position in the contact ellipse, and can be approximated using radius R and angular velocity ω.

$$\begin{aligned} v_s(y) &= v_d - \omega R(y) = v_d - \omega\sqrt{R^2 - y^2} \\ &\approx (v_d - \omega R) + \frac{\omega}{2R}y^2 \quad \text{. . . . . (7)} \end{aligned}$$

The approximation made in Eq. (7) is only valid for $y \ll R$, i.e., this becomes invalid in deep grooves of approximately equal radius as that of the ball. This assumption has been made with regard to the test bed used for the measurements.

This leads to following quadratic equation with the abbreviation ξ_0 for the starting value.

$$\xi(y) = \frac{v_s(y)}{v_d} = \xi_0 + \frac{1-\xi_0}{2R^2}y^2 \quad \text{. . . . . . . (8)}$$

The displacement of the bristles over the contact area is assumed to be a linear function, and can be calculated as follows.

$$u(x,y) = \xi(y)x + c \quad \text{. . . . . (9)}$$

To determine the constant of integration c, the following boundary condition must be considered: the entering bristles at the left boundary of the ellipse have no displacement.

$$c = \xi(y)\frac{a}{b}\sqrt{b^2 - y^2} \quad \text{. . . . . (10)}$$

The transition between stick and slip $a_0(y)$ occurs if the maximum displacement $u_{max}(y)$ of the bristle is reached, and it can be calculated as follows.

$$a_0(y) = \frac{-\xi(y)\frac{a}{b}\sqrt{b^2 - y^2} + \mathrm{sgn}(b_0 - y)u_{\max}}{\xi(y)} \quad \text{. (11)}$$

The condition $a_0(y = b) = 0$ can be recognized easily. Hence, the left boundary of the ellipse is to be used as the endpoint of the integration interval.

When the maximum force along the x-direction is reached, i.e., at the transition between stick and slip, the integral along x must be separated into two parts. The first integration interval is between the left ellipse boundary and a_0, and the second is between a_0 and the right boundary. Otherwise, it can be integrated along the whole ellipse.

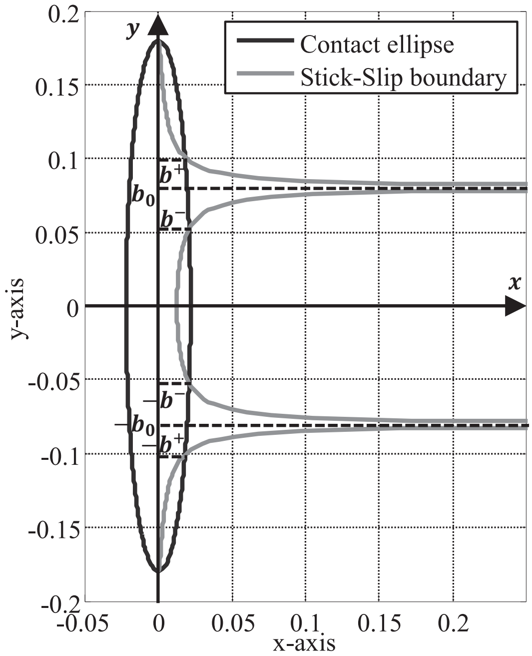

Fig. 3. Stick and slip areas in elliptical contact surface between the ball and raceway. The ball is moving leftwards. The dashed lines indicate the lines of pure rolling, and the gray line indicates the stick-slip transition.

To determine the intervals in the y-direction, the intersections between the contact ellipse and a_0 must be identified. Therefore, a_0 has to be equal to the right boundary of the ellipse. This results in two intersections b^- in area I and b^+ in area II. The first root of Eq. (12), namely y_I, becomes real only if such an intersection exists.

$$\begin{aligned} b^- = y_{\mathrm{I}} &= \sqrt{\frac{\left(-\xi_0 - \dfrac{3Q\mu}{4\pi a^2 b k_q}\right)2R^2}{1-\xi_0}} \qquad 0 \le y < b_0 \\ b^+ = y_{\mathrm{II}} &= \sqrt{\frac{\left(-\xi_0 + \dfrac{3Q\mu}{4\pi a^2 b k_q}\right)2R^2}{1-\xi_0}} \qquad b_0 \le y \le b \end{aligned} \quad \text{. . . . . (12)}$$

It is assumed that the points of pure rolling are on a circle with a radius ρ and a distance b_0 to the center of the ball. The levers h_I and h_{II}, which are respectively the z-distances from the instantaneous center of rotation to the distributed contact forces f_I and f_{II} displayed in **Fig. 1**, can be calculated as shown by Ito [1]. The signs must be regarded in this equation if they were not implied in the force.

$$\begin{aligned} h_{\mathrm{I}} &= \sqrt{\rho^2 - y^2} - \sqrt{\rho^2 - b_0^2} \qquad 0 \le y < b_0 \\ h_{\mathrm{II}} &= \sqrt{\rho^2 - b_0^2} - \sqrt{\rho^2 - y^2} \qquad b_0 \le y \le b \end{aligned} \quad \text{. (13)}$$

Figure 3 shows the integration boundaries. The contact ellipse, which determines the outer limits, is outlined in black, and the stick slip border, calculated by Eq. (9),

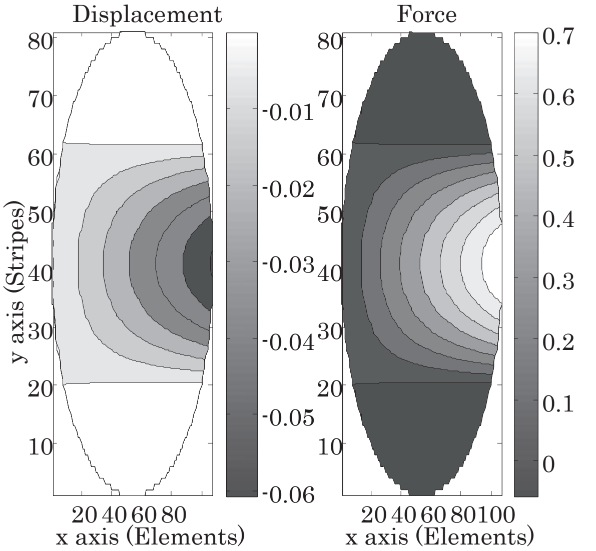

Fig. 4. Displacement (left side) and force (right side) caused by velocity difference in the contact ellipse are shown. Outside the contact ellipse, neither the displacement nor the force is calculated. The ball is moving leftwards.

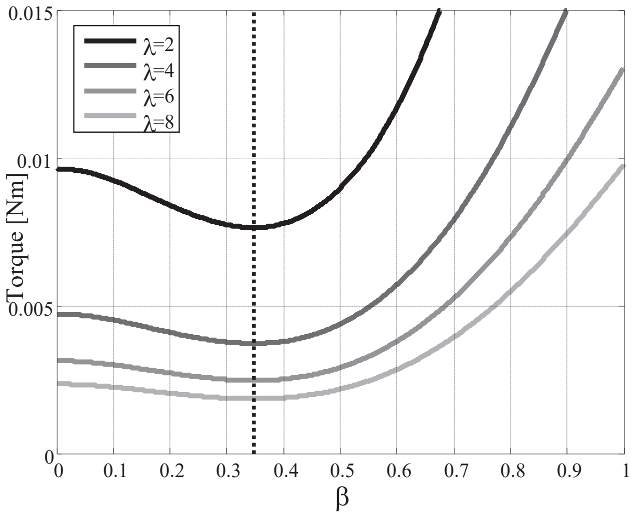

Fig. 5. The friction torque as a function of different values of the confined dimensionless parameters β and λ. For the chosen parameters, the minimum is located at $\beta \approx 0.347$, indicated by the dotted line.

is outlined in gray. The lines of pure rolling $\pm b_0$ are the singularities of Eq. (11). These can be easily identified, as there are no displacements between the ball and raceway at these lines. Consequentially, the force will be zero along these lines, and they do not intersect with the maximum force.

The estimated displacement and the related force in the contact area are shown in **Fig. 4**. In this example, the rolling element is moving in the left direction. Therefore, at the left boundary of the contact ellipse, both the displacement and the force are zero. They respectively increase and decrease until they reach the right boundary. Outside the contact ellipse, neither the displacement nor force is calculated.

3.2. Torque

With this information, the torque can be calculated. On grounds of symmetry, only the positive y-direction has to be calculated. However, the integrals have to be apportioned into all the four areas shown in **Fig. 3**. In the x-direction, the integrals must be calculated over the complete length of the contact ellipse depending on the y-position.

$$\begin{aligned} M = 2 \Bigg(& \int_0^{b^-} \int_{-a(y)}^{a_0(y)} F(x,y) h_{\mathrm{I}} \mathrm{d}x\mathrm{d}y \\ & + \int_{b^-}^{b_0} \int_{-a(y)}^{a(y)} F(x,y) h_{\mathrm{I}} \mathrm{d}x\mathrm{d}y \\ & + \int_{b_0}^{b^+} \int_{-a(y)}^{a(y)} F(x,y) h_{\mathrm{II}} \mathrm{d}x\mathrm{d}y \\ & + \int_{b^+}^{b} \int_{-a(y)}^{a_0(y)} F(x,y) h_{\mathrm{II}} \mathrm{d}x\mathrm{d}y \Bigg) \end{aligned} \quad (14)$$

The result provides the torque as a function of two parameters and representing the position of pure rolling lines b_0 and radius ρ, which are displayed in **Fig. 1**.

3.3. Estimation of Pure Rolling Lines

To estimate the position of pure rolling, the geometry-related variables must be substituted by independent parameters that can be limited within a defined interval. Here, β describes the position of the pure rolling line, which must take a value between zero and the major radius of the contact ellipse b. λ describes the relationship between the radius of the points of pure rolling ρ and the contact ellipse.

$$\begin{aligned} b_0 &= \beta b \qquad 0 \leq \beta \leq 1 \\ \rho &= \lambda b \qquad \lambda \geq 1 \end{aligned} \quad (15)$$

It is obvious that the pure rolling lines must be inside the contact ellipse; hence, b_0 must be lesser than b and the minimal radius ρ of a circle between the pure rolling lines is equal b.

The torque becomes minimal at the pure rolling lines. In the example shown in **Fig. 5**, these minima are located around $\beta \approx 0.347$, and the torque under variation of these parameters β and λ is calculated primarily at the minima, which describe the position of pure rolling. Obviously, these values are restricted to a very small range. If the other parameters such as preload, radii, or stiffness are changed, the positions of these minima will change, but they will remain within the small range.

Using this result, the starting value ξ_0 of the relative velocity can be calculated by the following equation.

$$\xi_0 = \frac{b_0^2}{b_0^2 - 2R^2} \quad (16)$$

Table 1. Numerical parameter for simulation.

Parameter	Value	Unit
Ball radius R	3.175	mm
Raceway radius R_r	3.5	mm
Normal force (one ball) Q	50	N
Young's modulus (ball) E_1	210000	N/mm^2
Young's modulus (raceway) E_2	205000	N/mm^2
Poisson's ration (ball) ν_1	0.3	
Poisson's ration (raceway) ν_2	0.25	
Carriage velocity v_d	10	mm/s
Rolling friction coefficient μ	0.001	
Slip exaggeration factor C_v	1.2	

3.4. Friction Hysteresis

As long as sticktion is existent, the displacement of the bristles increases linearly, as described in Eq. (9). However, there will be slipping if the maximum displacement is reached. In this case, the bristle displacement stays constant. The force along each stripe and the complete force in the contact can be calculated by integrating Eq. (1).

$$f_{\text{Stripe}}(y) = \int F(x,y)\mathrm{d}x$$
$$f_{\text{Complete}} = \iint F(x,y)\mathrm{d}x\mathrm{d}y \quad \quad (17)$$

4. Simulation Results and Verification

4.1. Simulation Parameters

In **Table 1**, the parameters used in the simulation are given. These contain geometry, material properties, external force, velocity, and some other parameters determined by experiments.

With these parameters, the contact area, pressure, and the position of pure rolling lines are determined.

4.2. Experimental Results

The test stand is a linear motor-driven, three-axis machine tool with a raceway mounted on the carriage. Therefore, the normal force can be set by the position of the z-axis. To minimize the influence of interaction between the balls, as well as the influence of distribution of balls' diameter, only four rolling elements are used. Three balls are necessary to avoid gearing, rolling, and pitching of the wagon, which might influence the measured force, but four have been chosen to obtain a symmetrical load distribution. To avoid reactive forces by geometrical and mounting aberrations, a joint is included between the z-axis and the force sensor. A schema of the test stand and rail raceway with four balls, which is mounted on the table, is displayed in **Fig. 6**.

The rolling friction coefficient μ describes the relationship between the normal and tangential forces. Its value depends on the contact surfaces. For bearings that are steel hardened and ground, $\mu \approx 0.001$ [19, 20].

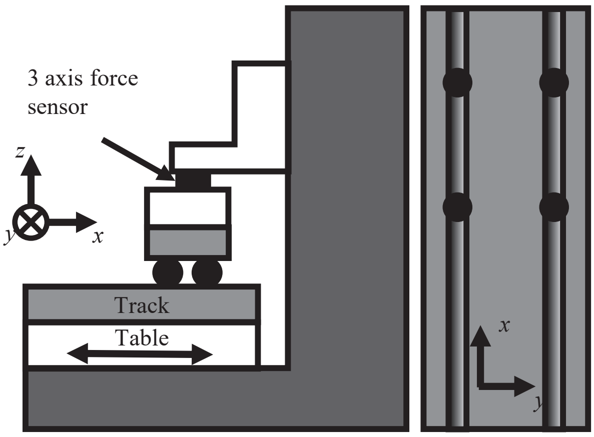

Fig. 6. Test stand and enlarged raceway with four rolling elements.

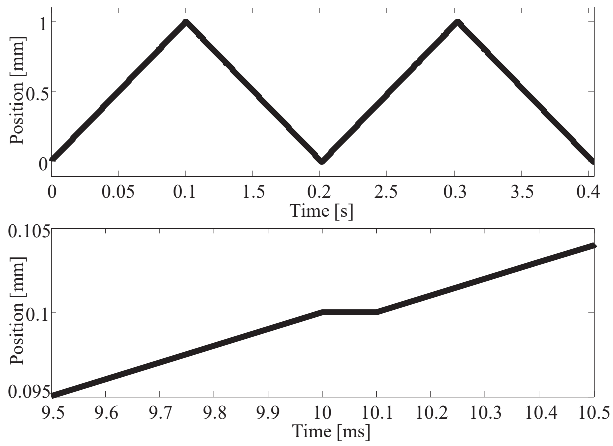

Fig. 7. The complete position profile (top) and the details of a stop (bottom).

Friction behavior of a ball was observed with the described test stand using the geometrical, material, force, and velocity parameters listed in **Table 1**.

The position profile used for the measurement and simulation is shown in **Fig. 7**. The axis is moved to the target position located at 1 mm in 0.1 mm steps and back with a constant velocity shown in the top part of the figure. However, to measure the maximum sticktion and the slipping force, stops are provided every 0.1 mm. Such a stop is shown by the constant position between Samples 100 and 101 in the bottom part of **Fig. 7**. Altogether, there are ten stops over the total length of the traveling distance during the measurement and simulation, as displayed in **Fig. 8**.

Figure 8 displays a typical measured friction hysteresis of a dry rolling contact, measured with the motion pattern shown in the top part of **Fig. 7**. The peaks represent the remaining force when the feed motion is stopped, as illustrated in the bottom part of **Fig. 7**. This implies that the peaks are the remaining sticktion force. The maximum sticktion force can be estimated easily; the exaggeration

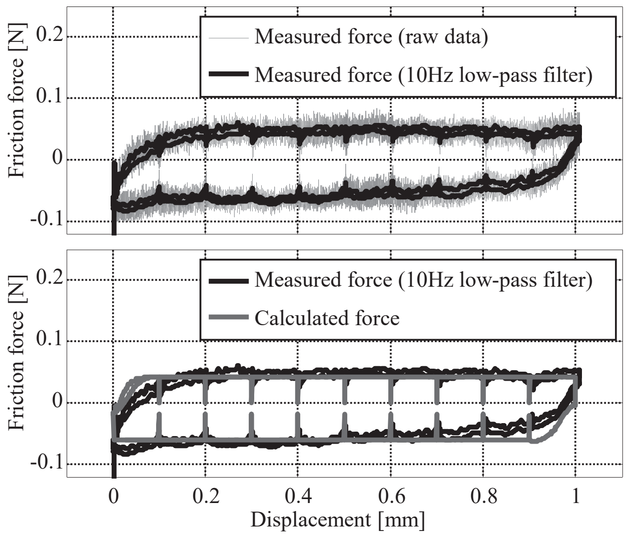

Fig. 8. The measured and filtered data (top) and comparison of filtered measurements and simulation results (bottom).

factor between the stick and slip is calculated by the variation in the force when the carriage is stopped and the contact stiffness is the slope of the hysteresis. This force variation is shown in **Fig. 8**.

4.3. Verification

The estimated parameters are used to calculate the contact area, pure rolling lines, and friction force. In the following **Fig. 8**, the measurement results of the described test stand are shown. The measurement was conducted without lubrication. Since there was considerable noise in the measured data, they were filtered with a 10-Hertz low pass filter. However, this significantly affected the sticktion peaks. Therefore, the slip exaggeration factor was estimated with the original data.

As apparent from the bottom of **Fig. 8**, the simulation result accurately applies to the filtered measurement, which describes the rolling friction force. Furthermore, the height of the simulated peaks, which represents the sticktion force, is equal to the measured peaks shown in the unfiltered curve (raw data), shown in the top part of **Fig. 8**. This implies that the developed model allows the estimation of both the sticktion force and rolling friction of a ball. However, there are still some discrepancies in the initiation of movement and change of direction. These might be induced by the reorientation processes at the contact surface, which are not considered in the model yet.

5. Conclusion

In this paper, a contact model based on Soda's friction model is developed and implemented to analyze a rolling contact in linear bearings. This model facilitates the determination of the lines of pure rolling, the differential velocity, and the friction force at the contact. This allows predicting of the measured friction behavior and the hysteresis caused by friction. Both stick and slip behaviors are observable through the measurements and simulation. Furthermore, the stick and slip areas in the contact surface can be estimated. Although it is a simple contact model, the theoretically estimated friction force significantly matches with the measured friction force.

In future, more realistic lubrication conditions such as grease or oil should be observed, and the time and velocity dependence of friction should be clarified. Thereafter, the number of rolling elements and the traveling distance should be increased to measure a more realistic system and to determine the influence of interactions between several rolling bodies. Finally, a complete linear bearing should be observed and modeled. With this model, friction compensation of high- and ultra-precision machine tools shall be improved. Furthermore, this approach can be used for modeling rotational bearings as well.

Acknowledgements

This research was supported by the Graduate School of advanced Manufacturing Engineering (GSaME) of the University of Stuttgart. This support is highly appreciated. Furthermore, we want to thank Dr. Iwao Yamaji for his assistance in arranging the measurements and configuring the test stand.

References:

[1] S. Ito, "Analysis of rolling friction between steel ball and raceway," Bearing Engineer, Vol.6, No.1, pp. 784-792, 1957 (in Japanese).

[2] T. Steinert, "Friction torque of ball bearings with retainer," Ph.D. Thesis, Rheinisch-Westfälische Technische Hochschule Aachen (RWTH Aachen), 1996 (in German).

[3] R. Teutsch, "Contact models and strategies for simulation of rolling bearings and linear motion guides," Ph.D. Thesis, University of Kaiserslautern, 2005 (in German).

[4] T. Fujita, A. Matsubara, and K. Yamazaki, "Experimental characterization of disturbance force in a linear drive system with high precision rolling guideways," Int. J. Mach. Tools Manuf., Vol.51, No.2, pp. 104-111, 2011.

[5] T. Tanaka, J. Otsuka, and T. Oiwa, "Precision positioning control by modeling frictional behaviors of linear ball guideway," Int. J. Automation Technol., Vol.3 No.3, pp. 334-342, 2009.

[6] F. Al-Bender, V. Lampaert, and J. Swevers, "The Generalized Maxwell-Slip Model: A Novel Model for Friction Simulation and Compensation," IEEE Trans. on Automatic Control, Vol.50, No.11, pp. 1883-1887, 2005.

[7] F. Al-Bender and W. Symens, "Characterization of frictional hysteresis in ball-bearing guideways," Wear, Vol.258, No.11-12, pp. 1630-1642, 2005.

[8] S. Futami, A. Furutani, and S. Yoshida, "Nanometer positioning and its micro-dynamics," Nanotechnology, Vol.1, No.1, pp. 31-37, 1990.

[9] B. Armstrong-Hélouvry, P. Dupont, and C. C. de Wit, "A Survey of Models, Analysis Tools and Compensation Methods for the Control of Machines with Friction," Automatica, Vol.30, No.7, pp. 1083-1138, 1994.

[10] A. Matsubara, A. Sayama, T. Sakai and M. Reuss, "Analysis of Measured Friction of Rolling Balls in Raceway Grooves," Int. J. Automation Technol., Vol.8, No.6, pp. 811-819, 2014.

[11] J. J. Kalker, "Three-Dimensional Elastic Bodies in Rolling Contact – Solid Mechanics and its Applications," Kluwer Academic publishers, pp. 28-34, 1990.

[12] K. L. Johnson, "Contact Mechanics," Cambridge University Press, pp. 84-106/p. 427, 1985.

[13] V. L. Popov, "Contact Mechanics and Friction – Physical Principles and Applications," Springer, Chapter 5, 2010.

[14] D.-F. Hu, Y.-H. Ji, and Y. Zhao, "Contact static stiffness research on machine tool considering the contact surface of rolling guideways," Mechatronics and Manufacturing Technologies: Proc. of the Int Conf. on Mechatronics and Manufacturing Technologies (MMT2016), pp. 196-203, 2016.

[15] T. Stolarski, "Tribology in Machine Design," Butterworth-Heinemann, pp. 249-250, 1999.

[16] N. Soda, Y. Kimura, and M. Sekizawa, "Wear occurring in rolling-sliding contact," Proc. of The Japan Society of Machine Tool Engineers, Vol.37, p. 2204, 1970 (in Japanese).

[17] Y. Kimura, M. Sekizawa, and A. Nitanai, "Wear and fatigue in rolling contact," Wear, Vol.253, No.1-2, pp. 9-16, 2002.

[18] T. Fujita, A. Matsubara, and S. Yamada, "Analysis of Friction in Linear Motion Rolling Bearing with Locomotive Multi-Bristle Model Influence of Slipping Velocity Distribution on Friction Characteristics," Trans. of The Japan Society of Mechanical Engineers, Vol.77, Issue 778, pp. 2486-2495, 2011 (in Japanese).

[19] W. Beitz, K.-H. Küttner, and B. J. Davis (Eds.), "Dubbel – handbook of mechanical engineering," Springer, p. E72, 1994 (in German).

[20] J. Awrejcewicz, "Classical Mechanics, Kinematics and Statics," Springer, p. 79, 2012.

Name:
Matthias Reuss

Affiliation:
Makino Milling Machine Co., Ltd.

Address:
4023 Nakatsu, Aikawa-machi, Aiko-gun, Kanagawa 243-0303, Japan

Brief Biographical History:
2008-2009 Engineer, Sodick Hightech
2009-2013 Researcher, Institute for Control Engineering of Machine Tools and Manufacturing Units, University of Stuttgart
2013-2018 Software Development Control Engineering, Industrielle Steuerungstechnik
2018- Advanced Development Section, Makino Milling Machine Co., Ltd.

Main Works:
• M. Reuss, A. Dadalau, and A. Verl, "Friction Variances of Linear Machine Tool Axes," Procedia CIRP, Proc. of the 3rd CIRP Conf. on Process Machine Interactions (3rd PMI), Vol.4, pp. 115-119, 2012.
• M. Reuss, "Reasons and impact of assembly variations on machine tools," J. of Advanced Mech. Design, Systems, and Manuf., Vol.10, No.5, JAMDSM0077, 2016.

Name:
Taku Sakai

Affiliation:
Kyoto Works, Mitsubishi Electric

Address:
1 Babazusyo, Nagaokakyo-shi, Kyoto 617-0828, Japan

Brief Biographical History:
2013- Design Engineer, Kyoto Works, Mitsubishi Electric

Membership in Academic Societies:
• Japan Society of Mechanical Engineers (JSME)

Name:
Atsushi Matsubara

Affiliation:
Professor, Department of Micro Engineering, Kyoto University

Address:
Katsura, Nishikyo-ku, Kyoto 615-8540, Japan

Brief Biographical History:
1992- Research Associate, Kyoto University
2002- Associate Professor, Kyoto University
2005- Professor, Kyoto University

Main Works:
• A. Matsubara, T. Yamazaki, and S. Ikenaga, "Non-contact measurement of spindle stiffness by using magnetic loading device," Int. J. Mach. Tools Manuf., Vol.71, pp. 20-25, 2013.
• A. Matsubara, K. Nagaoka, and T. Fujita, "Model-reference feedforward controller design for high-accuracy contouring control of machine tool axes," CIRP Ann. – Manuf. Technol., Vol.60, No.1, pp. 415-418, 2011.

Membership in Academic Societies:
• International Academy for Production Engineering (CIRP), Associate Member
• Japan Society for Precision Engineering (JSPE)
• Japan Society of Mechanical Engineers (JSME)
• Japan Society for Abrasive for Technology (JSAT)